

## **Biomass segregation between biofilm and flocs improves the control of nitrite-oxidizing bacteria in mainstream partial nitrification and anammox processes**

Laureni, Michele; Weissbrodt, David G.; Villez, Kris; Robin, Orlane; de Jonge, Nadieh; Rosenthal, Alex; Wells, George; Nielsen, Jeppe Lund; Morgenroth, Eberhard; Joss, Adriano

**DOI**

[10.1016/j.watres.2018.12.051](https://doi.org/10.1016/j.watres.2018.12.051)

**Publication date**

2019

**Document Version**

Final published version

**Published in**

Water Research

**Citation (APA)**

Laureni, M., Weissbrodt, D. G., Villez, K., Robin, O., de Jonge, N., Rosenthal, A., Wells, G., Nielsen, J. L., Morgenroth, E., & Joss, A. (2019). Biomass segregation between biofilm and flocs improves the control of nitrite-oxidizing bacteria in mainstream partial nitrification and anammox processes. *Water Research*, 154, 104-116. <https://doi.org/10.1016/j.watres.2018.12.051>

**Important note**

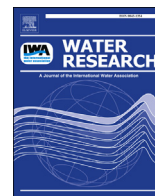
To cite this publication, please use the final published version (if applicable).  
Please check the document version above.

**Copyright**

Other than for strictly personal use, it is not permitted to download, forward or distribute the text or part of it, without the consent of the author(s) and/or copyright holder(s), unless the work is under an open content license such as Creative Commons.

**Takedown policy**

Please contact us and provide details if you believe this document breaches copyrights.  
We will remove access to the work immediately and investigate your claim.



# Biomass segregation between biofilm and flocs improves the control of nitrite-oxidizing bacteria in mainstream partial nitrification and anammox processes



Michele Laurenzi<sup>a, b, \*, 1, 2</sup>, David G. Weissbrodt<sup>c, d</sup>, Kris Villez<sup>a</sup>, Orlane Robin<sup>a</sup>, Nadieh de Jonge<sup>d</sup>, Alex Rosenthal<sup>e</sup>, George Wells<sup>e</sup>, Jeppe Lund Nielsen<sup>d</sup>, Eberhard Morgenroth<sup>a, b</sup>, Adriano Joss<sup>a</sup>

<sup>a</sup> Eawag: Swiss Federal Institute of Aquatic Science and Technology, Überlandstrasse 133, 8600, Dübendorf, Switzerland

<sup>b</sup> Institute of Environmental Engineering, ETH Zürich, Stefano-Franscini-Platz 5, CH-8093, Zürich, Switzerland

<sup>c</sup> Department of Biotechnology, Delft University of Technology, Van der Maasweg 9, NL- 2629, HZ Delft, the Netherlands

<sup>d</sup> Department of Chemistry and Bioscience, Aalborg University, Fredrik Bajers Vej 7H, DK-9220, Aalborg, Denmark

<sup>e</sup> Northwestern University, Department of Civil and Environmental Engineering, Evanston, IL, USA

## ARTICLE INFO

### Article history:

Received 20 October 2018

Received in revised form

24 December 2018

Accepted 27 December 2018

Available online 7 January 2019

### Keywords:

Mainstream anammox

Partial nitrification/anammox

Hybrid system

IFAS

Biomass segregation

NOB washout

Mathematical modelling

Nitrite sink

## ABSTRACT

The control of nitrite-oxidizing bacteria (NOB) challenges the implementation of partial nitrification and anammox (PN/A) processes under mainstream conditions. The aim of the present study was to understand how operating conditions impact microbial competition and the control of NOB in hybrid PN/A systems, where biofilm and flocs coexist. A hybrid PN/A moving-bed biofilm reactor (MBBR; also referred to as integrated fixed film activated sludge or IFAS) was operated at 15 °C on aerobically pre-treated municipal wastewater (23 mg<sub>NH4-N</sub> L<sup>-1</sup>). Ammonium-oxidizing bacteria (AOB) and NOB were enriched primarily in the flocs, and anammox bacteria (AMX) in the biofilm. After decreasing the dissolved oxygen concentration (DO) from 1.2 to 0.17 mg<sub>O2</sub> L<sup>-1</sup> - with all other operating conditions unchanged - washout of NOB from the flocs was observed. The activity of the minor NOB fraction remaining in the biofilm was suppressed at low DO. As a result, low effluent NO<sub>3</sub><sup>-</sup> concentrations (0.5 mg<sub>N</sub> L<sup>-1</sup>) were consistently achieved at aerobic nitrogen removal rates (80 mg<sub>N</sub> L<sup>-1</sup> d<sup>-1</sup>) comparable to those of conventional treatment plants. A simple dynamic mathematical model, assuming perfect biomass segregation with AOB and NOB in the flocs and AMX in the biofilm, was able to qualitatively reproduce the selective washout of NOB from the flocs in response to the decrease in DO-setpoint. Similarly, numerical simulations indicated that flocs removal is an effective operational strategy to achieve the selective washout of NOB. The direct competition for NO<sub>2</sub><sup>-</sup> between NOB and AMX - the latter retained in the biofilm and acting as a “NO<sub>2</sub>-sink” - was identified by the model as key mechanism leading to a difference in the actual growth rates of AOB and NOB (*i.e.*, μ<sub>NOB</sub> < μ<sub>AOB</sub> in flocs) and allowing for the selective NOB washout over a broad range of simulated sludge retention times (SRT = 6.8–24.5 d). Experimental results and model predictions demonstrate the increased operational flexibility, in terms of variables that can be easily controlled by operators, offered by hybrid systems as compared to solely biofilm systems for the control of NOB in mainstream PN/A applications.

© 2019 The Author(s). Published by Elsevier Ltd. This is an open access article under the CC BY-NC-ND license (<http://creativecommons.org/licenses/by-nc-nd/4.0/>).

## 1. Introduction

Partial nitrification and anammox (PN/A) is a resource-efficient alternative process for the removal of nitrogen from municipal wastewater (MWW) and holds promise to bring wastewater treatment plants (WWTP) close to neutral or even positive energy balances (Siegrist et al., 2008; van Loosdrecht and Brdjanovic,

\* Corresponding author. Eawag: Swiss Federal Institute of Aquatic Science and Technology, Überlandstrasse 133, 8600, Dübendorf, Switzerland.

E-mail addresses: [m.laurenzi@tudelft.nl](mailto:m.laurenzi@tudelft.nl), [mil@bio.aau.dk](mailto:mil@bio.aau.dk) (M. Laurenzi).

<sup>1</sup> Present address: Department of Biotechnology, Delft University of Technology, Van der Maasweg 9, NL- 2629 HZ Delft, The Netherlands.

<sup>2</sup> Present address: Department of Chemistry and Bioscience, Aalborg University, Fredrik Bajers Vej 7H, DK-9220 Aalborg, Denmark.

2014). PN/A technologies are implemented for the treatment of warm and concentrated streams such as digester supernatant (“sidestream PN/A”; Lackner et al. (2014)). Research targeting the direct application of PN/A to more dilute MWW, or “mainstream PN/A”, is progressing at a fast pace (De Clippeleir et al., 2013; Gilbert et al., 2015; Laureni et al., 2016; Lotti et al., 2015). The challenges associated with mainstream PN/A relate to the highly variable, dilute and cold characteristics of MWW. Moreover, mainstream PN/A must guarantee volumetric N-removal rates comparable to conventional WWTP (i.e.,  $100 \text{ mg}_N \text{ L}^{-1} \text{ d}^{-1}$ ; Metcalf et al. (2013)) and reliably discharge effluent to stringent water quality standards (e.g., below  $2 \text{ mg}_{\text{NH}_4\text{-N}} \text{ L}^{-1}$  in Switzerland; WPO (1998)).

Successful PN/A relies on the concerted activity of aerobic (AOB) and anaerobic ammonium-oxidizing (AMX) bacteria (Speth et al., 2016). Optimized microbial community engineering strategies are required to favour the growth of AOB and retain the slower-growing AMX, while out-competing the undesired nitrite-oxidizing bacteria (NOB). Several operational strategies implemented in sidestream applications are not feasible under mainstream conditions. At mesophilic temperatures ( $>20^\circ\text{C}$ ), AOB display higher maximum growth rates than NOB, which allows selective NOB washout at a sufficiently low solids retention time. Conversely, at mainstream temperatures between  $10$  and  $20^\circ\text{C}$  (in temperate regions), the differences in growth rates are minimal (Hellings et al., 1998). In addition, nitrogen concentrations in the main line are too low for NOB to be inhibited by free ammonia ( $\text{NH}_3$ ) or free nitrous acid ( $\text{HNO}_2$ ) (Anthonisen et al., 1976; Jubany et al., 2009). As a result, NOB control and washout cannot be based on maximum growth rates alone, as is efficiently achieved in sidestream suspended biomass systems (Hellings et al., 1998; Joss et al., 2011).

The use of biofilms, either grown on carrier material or in the form of granular bio-aggregates, has proven effective to achieve stable and resilient PN/A under mainstream conditions at laboratory scale (Gilbert et al., 2015; Laureni et al., 2016; Lotti et al., 2015). Biofilms allow for the long solids retention times (SRT) needed to retain AMX, while substrate gradients promote the suppression of NOB activity (Brockmann and Morgenroth, 2010; Gilbert et al., 2015; Laureni et al., 2016; Lotti et al., 2014; Pérez et al., 2014). NOB control in biofilm systems is mainly driven by the competition for oxygen with AOB, with the latter usually featuring higher substrate affinities (Brockmann and Morgenroth, 2010; Corbala-Robles et al., 2016; Pérez et al., 2014). PN/A operation under oxygen-limited  $\text{NH}_4^+$  oxidation can favour nitrification while limiting the aerobic growth of NOB (Brockmann and Morgenroth, 2010; Isanta et al., 2015; Pérez et al., 2014). However, operation under oxygen limitation inherently limits the AOB activity as well, and thus the overall process rate (Laureni et al., 2015; Pérez et al., 2014). Moreover, despite the generally accepted higher affinity of AOB for oxygen (Rittmann and McCarty, 2001), NOB are known to adapt to low dissolved oxygen concentrations (DO) (Liu and Wang, 2013), and several studies have recently reported higher oxygen affinities for NOB than AOB (Malovany et al., 2015; Regmi et al., 2014; Sliemers et al., 2005). Lastly, although their activity can be suppressed, NOB can persist in the biofilm and become active when favourable conditions are re-established, making their long-term suppression in solely biofilm systems challenging (Fux et al., 2004; Gilbert et al., 2015; Isanta et al., 2015; Laureni et al., 2016; Lotti et al., 2014).

Hybrid systems, where biofilms and flocs coexist (also referred to as integrated fixed film activated sludge or IFAS), are currently receiving increased attention for their potential advantages for PN/A applications. Experimental evidence (Laureni et al., 2016; Leix et al., 2016; Malovany et al., 2015; Park et al., 2014; Shi et al., 2016; Veuillet et al., 2014; Vlaeminck et al., 2010; Wells et al., 2017; Winkler et al., 2011) and numerical results (Hubaux et al.,

2015; Volcke et al., 2012) indicate that the faster-growing aerobic guilds tend to enrich in the floc fraction, with direct access to dissolved substrates. In turn, AMX have been shown to enrich in the biofilm, where anoxic conditions are achieved. As a result, differential control of the retention times of the bacterial guilds associated with the two biomass fractions is in principle possible (Wett et al., 2015). Moreover, as flocs are less diffusion-limited than biofilms, significantly higher aerobic volumetric conversion rates can be achieved even at low DO (Veuillet et al., 2014). Nonetheless, published data on hybrid systems operated for PN/A remain limited and seemingly contradictory. Hybrid systems at high flocs concentrations above  $1 \text{ g}_{\text{TSS}} \text{ L}^{-1}$  have been applied at full scale to treat digester supernatant at mesophilic temperatures with negligible NOB activity (Veuillet et al., 2014). Conversely, increased NOB activity has been reported in hybrid systems with a fraction of flocs as small as  $< 10\%$  of total solids (Hubaux et al., 2015; Laureni et al., 2016). The implications of biomass segregation and operational conditions for microbial competition in hybrid systems are as yet largely unknown.

The aim of this work was to understand the dominant mechanisms controlling the interaction between biofilm and flocs, the influence of operating conditions, and their implications for NOB control in hybrid PN/A systems. The effect of the DO on NOB was assessed experimentally in an IFAS system operated on real MWW at  $15^\circ\text{C}$ . In parallel, a simplified dynamic mathematical model of the hybrid system was developed to provide a mechanistic interpretation of the experimental results, and to understand how the composition of the flocs and the NOB concentration respond to changes in DO, flocs removal, and AMX activity in the biofilm. The sensitivity of the simulation outcome to model parameters was assessed. Relevant scenarios for engineering practice are also discussed.

## 2. Materials and methods

### 2.1. Long-term reactor operation at different DO

A 12 L hybrid MBBR was operated as a sequencing batch reactor (SBR) for PN/A on aerobically pre-treated MWW (see next section). The reactor was filled at a volumetric ratio of 33% with K5 biofilm carriers (AnoxKaldnes™, Sweden; protected surface of  $800 \text{ m}^2 \text{ m}^{-3}$ ). The biomass was previously acclimatised to the influent for over one year (Laureni et al., 2016). The reactor was run for 565 days at  $15.5 \pm 1.0^\circ\text{C}$ . Each SBR cycle consisted of six steps: feeding (5 L of pre-treated MWW, 5 min), anoxic mixing (10 min; 200 rpm), aeration and mixing (variable duration in the range 60–200 min; terminated at a residual  $\text{NH}_4^+$  concentration of  $2 \text{ mg}_{\text{NH}_4\text{-N}} \text{ L}^{-1}$ ), anoxic mixing (60 min), settling (60 min), and effluent discharge (terminated at 7 L fill level; 2 min). The DO was varied between micro-aerobic conditions (Phases I, III, V:  $0.17 \pm 0.04 \text{ mg}_{\text{O}_2} \text{ L}^{-1}$  (Gilbert et al., 2015)), and aerobic conditions (Phases II, IV:  $1.2 \pm 0.2 \text{ mg}_{\text{O}_2} \text{ L}^{-1}$  and  $1.6 \pm 0.1 \text{ mg}_{\text{O}_2} \text{ L}^{-1}$  (Regmi et al., 2014)) (Fig. 2). The total cycle duration varied between  $3.5 \pm 0.5$  and  $5.3 \pm 0.3$  h for operation at high and low DO, respectively.

The reactor was equipped with an optical oxygen sensor (Oxy-max COS61D), ion-selective electrodes for  $\text{NH}_4^+$  and  $\text{NO}_3^-$  concentrations, and pH and temperature sensors (ISEmax CAS40D), all from Endress + Hauser (Switzerland). The pH was not controlled and remained stable at  $7.4 \pm 0.2$  throughout the experimental period. Operational data are presented in Figure S1.

### 2.2. Municipal wastewater (MWW)

The municipal wastewater was taken from the sewer of Dübendorf (Switzerland). After primary treatment (screen, sand

removal and primary clarifier), MWW was pre-treated in an aerated 12 L SBR operated for high-rate organic carbon (as COD) removal at an SRT of 1 d. The pre-treated MWW featured the following characteristics:  $54 \pm 13 \text{ mg}_{\text{COD}_{\text{sol}}} \text{ L}^{-1}$ ,  $23 \pm 6 \text{ mg}_{\text{NH}_4\text{-N}} \text{ L}^{-1}$ , and  $<0.3 \text{ mg}_\text{N} \text{ L}^{-1}$  of  $\text{NO}_2^-$  and  $\text{NO}_3^-$ . Prior to feeding to the PN/A reactor, the pre-treated MWW was stored in a temperature-controlled ( $<20^\circ\text{C}$ ) external buffer tank of 50 L to equalize the hydraulic loads.

### 2.3. Control of total suspended solids (TSS) and calculation of their dynamic SRT

In addition to the settling step in the SBR cycle, from day 70 onwards the reactor effluent was filtered through a 10 L filter-bag (50- $\mu\text{m}$ -mesh; 3M™ NB Series, Nylon Monofilament) placed in a 50 L barrel. The content of the net was centrifuged for 5 min at  $2000 \times g$ , and the solids were reintroduced into the reactor on a daily basis. The TSS in the reactor and all activities were measured one cycle after biomass reintroduction.

The dynamic total SRT was calculated considering only the observed sludge loss in the effluent and by sampling (modified from Takács et al. (2008)):

$$\text{SRT}_{t+\Delta t} = \text{SRT}_t \left( 1 - \frac{X_{\text{effluent}} V_{\text{effluent}} + X_{\text{reactor}} V_{\text{sample}}}{X_{\text{reactor}} V_{\text{reactor}}} \right) + \Delta t \quad (1)$$

where  $X_{\text{effluent}}$  is the average TSS concentration in the filter-bag effluent ( $\text{g}_{\text{TSS}} \text{ L}^{-1}$ ),  $V_{\text{effluent}}$  is the total effluent volume discharged during the time interval,  $V_{\text{sample}}$  is the volume taken out for biomass sampling,  $X_{\text{reactor}}$  is the TSS concentration in the reactor ( $\text{g}_{\text{TSS}} \text{ L}^{-1}$ ),  $V_{\text{reactor}}$  is the volume of the bulk liquid phase in the reactor (12 L), and  $\Delta t$  is the time interval between subsequent measurements (d). The aerobic SRT is calculated from the total SRT as follows:

$$\text{SRT}_{\text{aerobic}} = \text{SRT} \frac{t_{\text{aerobic}}}{t_{\text{total}}} \quad (2)$$

where  $t_{\text{aerobic}}/t_{\text{total}}$  is the actual fraction of aerobic time over the total batch time (Fig. S1). The development of TSS, SRT and  $\text{SRT}_{\text{aerobic}}$  over time is presented in Fig. S2, together with the volumetric particle size distribution of the flocs measured on days 451 and 465 via laser light scattering (Mastersizer, 2000, Malvern, UK). During the experiment,  $\text{SRT}_{\text{aerobic}}$  increased from 4.7 to 49.1 days.

### 2.4. Maximum activities of AOB, NOB and AMX, and their segregation between biofilm and flocs

The maximum anammox activity ( $r_{\text{AMX,max}}$ ) is defined as the volumetric rate of nitrogen removal (sum of  $\text{NH}_4^+$  and  $\text{NO}_2^-$ ) in the absence of DO and under non-limiting concentrations of  $\text{NH}_4^+$  and  $\text{NO}_2^-$ .  $r_{\text{AMX,max}}$  was measured *in-situ* once or twice a week. The maximum activities of AOB and NOB ( $r_{\text{AOB,max}}$  and  $r_{\text{NOB,max}}$ ) are defined respectively as the volumetric rates of  $\text{NH}_4^+$  oxidation and  $\text{NO}_3^-$  production.  $r_{\text{AOB,max}}$  and  $r_{\text{NOB,max}}$  were measured via *ex-situ* batch tests (1 L) run under fully aerobic conditions ( $> 5 \text{ mg}_{\text{O}_2} \text{ L}^{-1}$ ) and non-limiting concentrations of  $\text{NH}_4^+$  and  $\text{NO}_2^-$ . The liquid fraction was sampled during mixing and a proportional number of random carriers were chosen manually. Mixing was provided with a magnetic stirrer (200 rpm) and the temperature was maintained at  $15 \pm 1^\circ\text{C}$ . After manually removing all carriers,  $r_{\text{AOB,max}}$  and  $r_{\text{NOB,max}}$  of the flocs were measured. The  $r_{\text{AMX,max}}$  value of the suspension was checked *ex-situ* five times throughout the experimental period and was confirmed to be negligible.  $\text{NH}_4^+$  and  $\text{NO}_2^-$  were supplied as

$\text{NH}_4\text{Cl}$  and  $\text{NaNO}_2$  ( $20\text{--}30 \text{ mg}_\text{N} \text{ L}^{-1}$ ), and volumetric consumption rates were calculated by linear regression of laboratory measurements of 3–4 grab samples from the bulk liquid phase.

### 2.5. Activities of AOB, NOB, and AMX during regular operation (aerobic step)

The volumetric activities of the three main autotrophic guilds during regular operation ( $r_{\text{AOB,cycle}}$ ,  $r_{\text{NOB,cycle}}$  and  $r_{\text{AMX,cycle}}$  expressed as  $\text{mg}_{\text{NH}_4\text{-N}} \text{ L}^{-1} \text{ d}^{-1}$ ,  $\text{mg}_{\text{NO}_3\text{-N}} \text{ L}^{-1} \text{ d}^{-1}$ , and  $\text{mg}_{(\text{NH}_4+\text{NO}_2)\text{-N}} \text{ L}^{-1} \text{ d}^{-1}$  respectively) were estimated according to Laurenzi et al. (2016). In short, during the aerated step of an SBR cycle, the consumption of  $\text{NH}_4^+$ , accumulation of  $\text{NO}_2^-$  and production of  $\text{NO}_3^-$  were followed by laboratory measurements of 3–4 grab samples from the bulk liquid phase. The activities were estimated based on the stoichiometric and kinetic matrix presented in Table 1, with parameters from Table 2. Heterotrophic denitrification during aeration was assumed to be negligible (Laurenzi et al., 2016).

### 2.6. Nitrogen removal over the entire SBR cycle and during the aerobic step

Over the entire SBR cycle, the volumetric N-removal rate ( $\text{mg}_\text{N} \text{ L}^{-1} \text{ d}^{-1}$ ) was calculated by dividing the difference between the sum of the dissolved nitrogen species ( $\text{NH}_4^+$ ,  $\text{NO}_2^-$  and  $\text{NO}_3^-$ ) in the influent and effluent by the hydraulic retention time (HRT, d). The relative removals (%) of  $\text{NH}_4^+$  and total nitrogen are defined as the difference between their influent and effluent concentrations divided by the influent concentrations. The influent and effluent were sampled once per week (Fig. S3).

During aeration, the aerobic volumetric N-removal rate ( $\text{mg}_\text{N} \text{ L}^{-1} \text{ d}^{-1}$ ) was calculated as the difference between the  $\text{NH}_4^+$  consumption rate and the rates of  $\text{NO}_2^-$  and  $\text{NO}_3^-$  production. The aerobic N-removal efficiency (%) was estimated by dividing the N-removal rate during aeration by the  $\text{NH}_4^+$  depletion rate.

### 2.7. Growth rate of AOB, NOB, and AMX

The maximum growth rates of AOB ( $\mu_{\text{AOB,max}}$ ) and NOB ( $\mu_{\text{NOB,max}}$ ) were estimated during Phase II, when substrate limitations were minor, based on the measured exponential increase in their maximum activity in the flocs ( $r_{i,\text{max}}$ , Fig. 2b), or in their activity during operation ( $r_{i,\text{cycle}}$ , Fig. 2c). Most of the activity increase occurred in suspension, where diffusion limitation was assumed to be of minor importance. The potential seeding of AOB and NOB from the biofilm was neglected. The suspended solids mass balance ( $X_i$ , with  $i = \text{AOB, NOB}$ ) is expressed as:

$$\frac{dX_i}{dt} = \left( \mu_{i,\text{max}} - b_i - \frac{1}{\text{SRT}} \right) X_i = \mu_{i,\text{obs}} X_i \quad (3)$$

where  $\mu_{i,\text{max}}$  and  $\mu_{i,\text{obs}}$  are the maximum and observed growth rates, respectively, of the guild  $i$  ( $\text{d}^{-1}$ ),  $b_i$  is the decay rate of the guild  $i$  ( $\text{d}^{-1}$ ; set to  $0.05 \mu_{i,\text{max}}$ ), and SRT is the solids retention time (d). The value of  $\mu_{i,\text{obs}}$  was obtained from the exponential interpolation of the measured increase in activities ( $r_i$ ,  $\text{mg}_\text{N} \text{ L}^{-1} \text{ d}^{-1}$ ):

$$r_{i,t} = r_{i,t-\Delta t} \exp(\mu_{i,\text{obs}} \Delta t) \quad (4)$$

From Eqs. (3) and (4), and considering that growth occurs only during the aerobic time, the maximum growth rate can be estimated as follows:



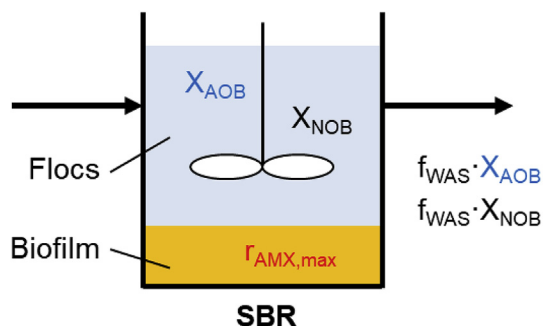


**Fig. 1.** Location of the active biomass in the mathematical model of the hybrid system. The model assumes perfect biomass segregation, with AOB and NOB in the flocs and AMX in the biofilm.  $r_{AMX,max}$  is the maximum volumetric anammox activity ( $\text{mg}_{(\text{NH}_4+\text{NO}_2)\text{-N}} \text{L}^{-1} \text{d}^{-1}$ ).  $f_{WAS}$  represents the fraction of flocs removed at the end of each SBR cycle.

$$\mu_{i,max} = (\mu_{i,obs} + b_i) \frac{t_{total}}{t_{aerobic}} + \frac{1}{SRT_{aerobic}} \quad (5)$$

where  $t_{aerobic}/t_{total}$  is the average fraction of aerobic time over the total batch time, and  $SRT_{aerobic}$  the average aerobic SRT during the considered period. The SRT was not considered in the estimation of the maximum growth rate of AMX ( $\mu_{AMX,max}$ ), as their growth occurred almost exclusively on the biofilm. The uncertainty associated with  $\mu_{i,max}$  was quantified by means of Monte Carlo simulations as previously described (Laureni et al., 2015).

### 2.8. Amplicon sequencing analyses of the bacterial community compositions in biofilm and flocs

The amplicon sequencing method is presented in the Supporting Information, Section S1.

### 2.9. Analytical methods

The concentration of  $\text{NH}_4^+$  was analysed using a flow injection analyser (FIStar 5000, Foss, Denmark). The concentrations of  $\text{NO}_2^-$  and  $\text{NO}_3^-$  were analysed by ion chromatography (Compact IC 761, Metrohm, Switzerland). The COD was measured photometrically with test kits (Hach Lange, Germany). The samples were filtered using  $0.45 \mu\text{m}$  filters (Macherey-Nagel, Germany) prior to analysis. The concentration of total and volatile suspended solids (VSS, TSS) in the mixed liquors was determined according to standard methods (APHA, 2005). The total solids (TS) on biofilm carriers were estimated as described previously (Laureni et al., 2016).

## 3. Mathematical model of the hybrid system

### 3.1. Model description

A dynamic model of the hybrid MBBR operated in SBR mode was developed and implemented in MATLAB (version R2015b, MathWorks Inc.). The MATLAB scripts are available as open-source code in the Supporting Information. The aim of the model was to understand how the composition of the flocs and the NOB concentration respond to changes in DO, fraction of flocs removed per SBR cycle ( $f_{WAS}$ ), and maximum volumetric AMX activity ( $r_{AMX,max}$ ). To this end, perfect biomass segregation was assumed, with AOB and NOB in the flocs and AMX in the biofilm (Fig. 1).

Five soluble compounds were considered: ammonium ( $\text{NH}_4^+$ ), nitrite ( $\text{NO}_2^-$ ), nitrate ( $\text{NO}_3^-$ ), di-nitrogen gas ( $\text{N}_2$ ), and DO.

The AOB, NOB, and AMX processes were modelled according to the stoichiometric and kinetic matrix in Table 1. Unless explicitly

stated, parameter values were taken from the literature (Table 2).  $X_{AOB}$  and  $X_{NOB}$  were assumed to grow in the flocs, and their abundance and activity to be influenced by growth and washout. For the sake of simplicity, the model excluded decay processes. Free ammonia and free nitrous acid inhibitions were considered negligible under mainstream concentrations and pH.

AMX were considered to grow in a deep biofilm (Morgenroth, 2008). The primary goal of the modelling was to understand the role of the biofilm as “ $\text{NO}_2^-$ -sink”: the biofilm was consequently modelled as zero-dimensional, and spatial gradients were neglected. In order to discuss the potential effects of diffusion, additional simulations were run with 10-fold increased values for  $\text{NO}_2^-$  and  $\text{NH}_4^+$  affinity constants of AMX. Moreover, as the activity of deep biofilms is transport-limited rather than biomass-limited, the maximum AMX process rate ( $\rho_{AMX,max} = \mu_{AMX,max} \cdot X_{AMX}$ ,  $\text{mg}_{\text{COD}} \text{L}^{-1} \text{d}^{-1}$ ; Table 1) was assumed to be constant during each simulation. This was implemented by considering the concentration of AMX ( $X_{AMX}$ ) and the process rate as constants. The oxygen inhibition of AMX was not explicitly modelled: deep biofilms are in fact oxygen-limited, and the modelled AMX activity is to be considered the activity resulting from the anoxic biofilm layers. For consistency with the experimental part, the simulation results are presented as a function of  $r_{AMX,max}$  ( $\text{mg}_{(\text{NH}_4+\text{NO}_2)\text{-N}} \text{L}^{-1} \text{d}^{-1}$ ) as obtained by the product of  $\rho_{AMX,max}$  and the sum of the stoichiometric coefficients for  $\text{NH}_4^+$  and  $\text{NO}_2^-$  (Table 1).

### 3.2. Simulation strategy and scenario analysis

The influent was assumed to contain  $20 \text{ mg}_{\text{NH}_4\text{-N}} \text{L}^{-1}$  and be devoid of  $\text{NO}_2^-$ ,  $\text{NO}_3^-$ , and COD. Filling, settling, and decanting steps were assumed to be instantaneous. Only the aerated phase was simulated dynamically. As in the operation of the experimental reactor, settling was initiated each time the  $\text{NH}_4^+$  concentration equalled  $2 \text{ mg}_{\text{N}} \text{L}^{-1}$ ; this resulted in variable cycle durations depending on biomass activity. Simulations were performed for a temperature of  $15^\circ\text{C}$  at which maximum growth rates were estimated in the reactor. The DO was assumed constant, and the volumetric exchange of MWW was 50% per cycle. The initial concentration of  $\text{NH}_4^+$  at the start of each cycle was the result of mixing (half of its value at the end of the previous cycle plus half of the influent concentration, i.e.,  $11 \text{ mg}_{\text{N}} \text{L}^{-1}$ ). The  $\text{NO}_2^-$  and  $\text{NO}_3^-$  concentrations at the start of each simulated cycle were always equal to half of their values at the end of the previous cycle. A fixed fraction of flocs ( $f_{WAS}$ ) was removed at the end of each cycle.  $f_{WAS}$  was defined as the mass removed from the reactor divided by mass of solids present in the reactor,  $(X_{removed} \cdot V_{removed}) / (X_{reactor} \cdot V_{reactor})$ . Simulations were run until a pseudo steady-state was reached, i.e., constant effluent N and flocs concentration. Pseudo steady-state were shown to be independent from the initial  $X_{AOB}$  and  $X_{NOB}$ . The sensitivity of the model outputs was assessed with respect to the ratio between the  $\text{O}_2$  affinity constants of NOB and AOB ( $K_{\text{O}_2,\text{NOB}}/K_{\text{O}_2,\text{AOB}}$ ) and the ratio between the  $\text{NO}_2^-$  affinity constants of NOB and AMX ( $K_{\text{NO}_2,\text{NOB}}/K_{\text{NO}_2,\text{AMX}}$ ) (Table S1; Figure S9).

A combination of different  $\rho_{AMX,max}$  ( $0\text{--}24 \text{ mg}_{\text{COD}} \text{L}^{-1} \text{d}^{-1}$ ; corresponding to  $r_{AMX,max}$   $0\text{--}300 \text{ mg}_{(\text{NH}_4+\text{NO}_2)\text{-N}} \text{L}^{-1} \text{d}^{-1}$ ), and  $f_{WAS}$  ( $0.4\text{--}1.7\%$ ) were simulated for two DO ( $0.15$  and  $1.5 \text{ mg}_{\text{O}_2} \text{L}^{-1}$ ). These modelled parameter values were explicitly chosen to fall in the range of the experimental values. To assess the impact of the individual control parameters, four specific scenarios are discussed (Table 3).

### 3.3. Interdependence between $f_{WAS}$ , HRT, and SRT

For an SBR where the reaction phase of the cycle is always extended until the target effluent  $\text{NH}_4^+$  concentration is reached ( $2 \text{ mg}_{\text{N}} \text{L}^{-1}$ ), the HRT, the  $f_{WAS}$ , and ultimately the SRT are

**Table 1**  
Stoichiometric and kinetic matrix describing the growth of aerobic ammonium-oxidizing bacteria (AOB) and aerobic nitrite-oxidizing bacteria (NOB), and anaerobic ammonium-oxidizing bacteria (anammox, AMX). The matrix was used to estimate the activity of the three guilds during regular SBR operation ( $r_{i,cycle}$ ), and for the dynamic model of the hybrid system (Fig. 1). In the dynamic model, the maximum anammox process rate ( $\rho_{AMX,max} = \mu_{AMX,max} \cdot X_{AMX}$ ) was assumed constant during each simulation. To this end, the concentration of AMX ( $X_{AMX}$ ) was considered as a constant and not as a state variable, and is therefore omitted from the matrix.

Component	$S_{O_2}$ $g_{O_2} m^{-3}$	$S_{NH_4}$ $g_N m^{-3}$	$S_{NO_2}$ $g_N m^{-3}$	$S_{NO_3}$ $g_N m^{-3}$	$S_{N_2}$ $g_N m^{-3}$	$X_{AOB}$ $g_{COD} m^{-3}$	$X_{NOB}$ $g_{COD} m^{-3}$	Process rates ( $\rho$ ) $g_{COD} m^{-3} d^{-1}$
<b>Processes (growth)</b>								
AOB	$-\frac{(3.43 - Y_{AOB})}{Y_{AOB}}$	$-\frac{1}{Y_{AOB}} - i_{N,AOB}$	$\frac{1}{Y_{AOB}}$			1		$\mu_{AOB,max} X_{AOB} \frac{S_{NH_4}}{S_{NH_4} + K_{AOB,NH_4}} \frac{S_{O_2}}{S_{O_2} + K_{AOB,O_2}}$
NOB	$-\frac{(3.43 - Y_{AOB})}{Y_{AOB}}$	$-i_{N,NOB}$	$-\frac{1}{Y_{NOB}}$	$\frac{1}{Y_{NOB}}$			1	$\mu_{AOB,max} X_{AOB} \frac{S_{NH_4}}{S_{NH_4} + K_{AOB,NH_4}} \frac{S_{O_2}}{S_{O_2} + K_{AOB,O_2}}$
AMX		$-\frac{1}{Y_{AMX}} - i_{N,AMX}$	$-\frac{1}{Y_{AMX}}$	$\frac{1}{1.14}$	$\frac{1}{1.14}$	$\frac{2}{Y_{AMX}}$		$\rho_{AMX,max} \frac{S_{NH_4}}{S_{NH_4} + K_{AMX,NH_4}} \frac{S_{NO_2}}{S_{NO_2} + K_{AMX,NO_2}}$
<b>Composition Matrix</b>								
gTOD	-1		-3.43	-4.57	-1.71	1	1	
gN		1	1	1	1	$i_{N,AOB}$	$i_{N,NOB}$	

**Table 2**  
Kinetic and stoichiometric parameters.

<b>Aerobic ammonium-oxidizing bacteria (AOB)</b>				
$\mu_{AOB,max}$	$d^{-1}$	Maximum specific growth rate	0.30	<i>This study*</i>
$Y_{AOB}$	$g_{COD} g_N^{-1}$	Growth yield	0.18	Jubany et al. (2009)
$K_{NH_4,AOB}$	$g_{NH_4-N} m^{-3}$	Ammonium half-saturation constant	2.4	(Wiesmann, 1994)
$K_{O_2,AOB}$	$g_{COD} m^{-3}$	Oxygen half-saturation constant	0.6	(Wiesmann, 1994)
$i_{N,AOB}$	$g_N g_{COD}^{-1}$	Nitrogen content in AOB	0.083	Volcke et al. (2012)
<b>Aerobic nitrite-oxidizing bacteria (NOB)</b>				
$\mu_{NOB,max}$	$d^{-1}$	Maximum specific growth rate	0.34	<i>This study*</i>
$Y_{NOB}$	$g_{COD} g_N^{-1}$	Growth yield	0.08	Jubany et al. (2009)
$K_{O_2,NOB}$	$g_{COD} m^{-3}$	Oxygen half-saturation constant	0.4	(Blackburne et al., 2007)
$K_{NO_2,NOB}$	$g_{NO_2-N} m^{-3}$	Nitrite half-saturation constant	0.5	(Wiesmann, 1994)
$i_{N,NOB}$	$g_N g_{COD}^{-1}$	Nitrogen content in NOB	0.083	Volcke et al. (2012)
<b>Anaerobic ammonium-oxidizing bacteria (AMX)</b>				
$\rho_{AMX,max}$	$mg_{COD} L^{-1} d^{-1}$	Maximum AMX process rate	0–24	Assumed**
$Y_{AMX}$	$g_{COD} g_N^{-1}$	Growth yield	0.17	(Strous et al., 1998)
$K_{NH_4,AMX}$	$g_{NH_4-N} m^{-3}$	Ammonium half saturation constant	0.03	Volcke et al. (2012)
$K_{NO_2,AMX}$	$g_{NO_2-N} m^{-3}$	Nitrite half saturation constant	0.005	Volcke et al. (2012)
$i_{N,AMX}$	$g_N g_{COD}^{-1}$	Nitrogen content in AMX	0.058	Volcke et al. (2012)

\*Estimated from the maximum activity increase at 15 °C during Phase II (Fig. 2a).

\*\* Corresponding to  $\Gamma_{AMX,max}$  in the range observed experimentally at 15 °C, 0–300  $mg_{(NH_4+NO_2)-N} L^{-1} d^{-1}$ .

interdependent. At pseudo steady-state, the AOB removed at the end of each cycle must equal the growth of AOB during that cycle:

$$SRT \approx \frac{X V_{reactor}}{(f_{WAS} X V_{reactor})/T} \approx \frac{T}{f_{WAS}} \approx \frac{1}{\mu_{AOB}} \quad (8)$$

From Eq. (8), after substituting Eq. (7), it can be seen that the SRT is not an independent parameter either, but is directly determined by the actual growth rate of the AOB for the given environmental conditions.

## 4. Results and discussion

### 4.1. Long term operation of the hybrid MBBR, and the impact of DO on NOB control

#### 4.1.1. Maximum volumetric activities ( $r_{i,max}$ ) segregation between biofilm and flocs

A 12-L hybrid MBBR was operated for mainstream PN/A at 15 °C on aerobically pre-treated MWW, and the impact of the DO on

**Table 3**  
Values of the control parameters for the four tested scenarios.

Scenario	DO $mg_{O_2} L^{-1}$	$f_{WAS}$ %	$\Gamma_{AMX,max}$ $mg_N L^{-1} d^{-1}$
1 (baseline)	1.5	0.5	86
2	<b>0.15</b>	0.5	86
3	1.5	<b>1.7</b>	86
4	1.5	0.5	<b>270</b>

$$f_{WAS} X_{AOB}(T) V_{reactor} = \int_{\tau=0}^T \mu_{AOB}(\tau) X_{AOB}(\tau) V_{reactor} d\tau \quad (6)$$

where  $X_{AOB}(T)$  is the concentration of AOB at the end of a cycle ( $mg_{COD} L^{-1}$ ),  $T$  is the length of the cycle (d),  $V_{reactor}$  is the working volume of the reactor (L),  $\mu_{AOB}(\tau)$  is the actual growth rate of AOB at time  $\tau$  during the cycle ( $d^{-1}$ ), and  $X_{AOB}(\tau)$  is the AOB concentration at time  $\tau$  ( $mg_{COD} L^{-1}$ ). Under the simplifying assumption that over a cycle  $\mu_{AOB} \approx const.$  and  $X_{AOB} \approx const.$ , Eq. (6) can be simplified to

$$f_{WAS} \approx \mu_{AOB} T \quad (7)$$

From Eq. (7) it can be seen that the HRT and the cycle time are directly linked: for a given actual growth rate of AOB, increasing  $f_{WAS}$  increases  $T$ , and thus the HRT. As a result, HRT and  $f_{WAS}$  cannot be controlled independently. The value of  $f_{WAS}$  also impacts the pseudo steady-state  $X_{AOB}$  and  $X_{NOB}$ , and lower biomass concentrations result from higher  $f_{WAS}$ . Furthermore, this has direct implications on the SRT of the flocs, defined as the average biomass present in the reactor divided by the biomass removed per cycle. Under the simplifying assumption that  $X \approx const.$  over a cycle, it follows that

microbial competition and NOB control was investigated. The total and flocs-associated maximum volumetric activities ( $r_{i,max}$ ) of the three main guilds were measured as proxy for their abundance (Fig. 2a and b).

Over more than one year the reactor was stably operated as PN/A (i.e. prior to Phase I in Fig. 2 (Laureni et al., 2016)). During Phase II, as a result of the simultaneous increase in DO from 0.17 to 1.2 mgO<sub>2</sub> L<sup>-1</sup> and the improved flocs retention,  $r_{AOB,max}$  and  $r_{NOB,max}$  increased exponentially (Fig. 2b). The observed increase was mainly associated with the flocs (dotted line in Fig. 2b). Over the same period, the total suspended solids increased from 0.2 to 1 gTSS L<sup>-1</sup> (Figure S2). The estimated maximum growth rate of AOB ( $\mu_{AOB,max}$ ) and NOB ( $\mu_{NOB,max}$ ) were  $0.30 \pm 0.06$  and  $0.34 \pm 0.06$  d<sup>-1</sup>, respectively. For AMX, a  $\mu_{AMX,max}$  of  $0.014 \pm 0.004$  d<sup>-1</sup> was estimated.

The increase in  $r_{AOB,max}$  and  $r_{NOB,max}$  stopped when the DO was decreased to its initial value of 0.17 mgO<sub>2</sub> L<sup>-1</sup> (day 115, Phase III) while keeping all other operational conditions unchanged. After an apparent delay of over six weeks,  $r_{NOB,max}$  started to decrease while the established  $r_{AOB,max}$  was maintained in the system (Fig. 2b). The loss in  $r_{NOB,max}$  was primarily associated with the flocs.

During Phase IV,  $r_{AOB,max}$  and  $r_{NOB,max}$  increased exponentially, in particular when the DO was increased to 1.6 mgO<sub>2</sub> L<sup>-1</sup> (day 460). Unfortunately, the increase stopped on day 475, when a dramatic drop in all  $r_{i,max}$  was observed in correlation with a multiple-day heavy rain event. This also coincided with a 15 % loss of TSS in the system, although this alone cannot explain the activity loss. Importantly, all  $r_{i,max}$  naturally recovered in less than two months (Phase V, Fig. 2). All operational conditions are presented in Figure S1.

#### 4.1.2. Volumetric activities during regular operation ( $r_{i,cycle}$ )

The actual volumetric activities ( $r_{i,cycle}$ ) of the three main guilds were measured during the aerobic step of an SBR cycle to assess the impact of the imposed operational condition on microbial competition. Actual activities are presented in Fig. 2c, and the observed yields of NH<sub>4</sub><sup>+</sup> converted to NO<sub>2</sub><sup>-</sup> and NO<sub>3</sub><sup>-</sup> are displayed in Fig. 2d.

During periods of high DO (Phase II and IV), the volumetric activities during regular operation ( $r_{i,cycle}$ ) were comparable to the maximum activities ( $r_{i,max}$ ), indicating that substrate limitations were minor under these conditions (Fig. 2a, c). The  $\mu_{AOB,max}$  ( $0.28 \pm 0.05$  d<sup>-1</sup>) and  $\mu_{NOB,max}$  ( $0.30 \pm 0.06$  d<sup>-1</sup>), estimated during Phase II, were in good agreement with those obtained from the increase in  $r_{i,max}$ .

Decreasing the DO on day 115 (Phase III) resulted in an immediate decrease of  $r_{AOB,cycle}$  and  $r_{NOB,cycle}$ , as both guilds become DO limited (Fig. 2c). After a delay of about two months,  $r_{NOB,cycle}$  started to decrease progressively in accordance with the behaviour of  $r_{NOB,max}$ . The decrease in  $r_{NOB,cycle}$  coincided with the increase of  $r_{AMX,cycle}$ , indicating a progressive shift in the competition for NO<sub>2</sub><sup>-</sup>. From day 285 onwards, very little NOB activity was detected as supported by the low NO<sub>3</sub><sup>-</sup> production. The slight NO<sub>2</sub><sup>-</sup> accumulation indicated an excess of  $r_{AOB,cycle}$  over the available  $r_{AMX,cycle}$  (Fig. 2d).

The increase in DO on day 375 (Phase IV) led to a sharp increase in  $r_{AOB,cycle}$  and lead, due to the excess AOB maintained in the system, to a pronounced accumulation of NO<sub>2</sub><sup>-</sup> to about 60% of the consumed NH<sub>4</sub><sup>+</sup> (Fig. 2d). The  $r_{NOB,cycle}$  also increased immediately, due to the NOB persisting in the biofilm, and NO<sub>3</sub><sup>-</sup> started to accumulate. The exponential increase of  $r_{AOB,cycle}$  and  $r_{NOB,cycle}$  stopped on day 475 in conjunction with the heavy rain event (Fig. 2c, empty arrow).

#### 4.1.3. Bacterial community composition of biofilm and flocs

The relative read abundances of AOB, NOB, and AMX in the biofilm and flocs are presented in Fig. 3. The dynamics of all

individual OTUs detected within the three guilds are shown in Figure S4. In good agreement with the observed  $r_{AMX,max}$ , AMX were almost exclusively present in the biofilm with relative abundances of up to 15% of the total reads (< 0.1% in suspension). Interestingly, four different OTUs were detected for AMX in the biofilm and displayed different dynamics, suggesting possible fine-scale differentiation in the “*Ca. Brocadia*” lineage. Fluorescence *in situ* hybridization (FISH) micrographs of biofilm cryosections are shown in Figure S7.

Significantly lower relative read abundances were observed for AOB and NOB throughout the entire operation (Fig. 3b and c). During Phase III, the TSS increased from 1 to over 2.5 gTSS L<sup>-1</sup> (Figure S2). The relative abundance of AOB (genus *Nitrosomonas*) progressively increased from approximately 0.5 to over 2.5% in the flocs, whereas the relative abundance of NOB (genus *Nitrospira*) decreased progressively from 0.4 to below 0.1%. Thus, the observed loss of NOB activity (Fig. 2) coincided with the actual washout of NOB from the flocs. The relative read abundances of both AOB and NOB guilds during Phase IV increased markedly on the biofilm, supporting the observed increases in  $r_{AOB,max}$  and  $r_{NOB,max}$  (Fig. 2). Two different OTUs were identified for AOB with distinct trends in biofilm and flocs.

The ratio of the relative read abundances of AOB and NOB is shown in Fig. 3d. AOB were selectively enriched over NOB in the flocs during the period at low DO (Phase III); the AOB/NOB ratio increased from 5 to over 20. No major changes in the AOB/NOB ratio were observed in the biofilm.

#### 4.1.4. NOB control at low DO: wash-out from the flocs and activity suppression in the biofilm

AOB and NOB grew in the flocs and biofilm. The enrichment of both guilds in the flocs, less diffusion-limited, is in good agreement with previous experimental and modelling reports on PN/A (Hubaux et al., 2015; Park et al., 2014; Veuillet et al., 2014; Vlaeminck et al., 2010; Volcke et al., 2012; Winkler et al., 2011). Also, AOB and NOB displayed comparable maximum specific growth rates as expected at mainstream temperatures (Hellinga et al., 1998). In principle, these conditions would hinder the possibility to differentiate the actual growth rates of the two guilds and selectively wash out NOB as efficiently achieved in sidestream suspended biomass systems (Hellinga et al., 1998; Joss et al., 2011). Nevertheless, prolonged operation at low DO (0.17 mgO<sub>2</sub> L<sup>-1</sup>) did result in the selective wash out of NOB from the flocs (Fig. 2). This is explained by a distinctive characteristic of hybrid systems, namely the competition for NO<sub>2</sub><sup>-</sup> between the NOB in the flocs and the AMX enriched in the biofilm acting as a “NO<sub>2</sub>-sink”. The proposed mechanisms for the selective NOB washout are extensively discussed in the modelling section.

The accumulation and persistence of an NOB fraction in biofilms has also been widely reported, and makes the suppression of NO<sub>2</sub><sup>-</sup> oxidation challenging in solely biofilm PN/A systems (Fux et al., 2004; Gilbert et al., 2015; Isanta et al., 2015; Lotti et al., 2014; Park et al., 2014; Poot et al., 2016; Veuillet et al., 2014). Here, the actual nitrification activity of the NOB ( $r_{NOB,cycle}$ ) in the biofilm was consistently controlled by the DO, and was completely suppressed at 0.17 mgO<sub>2</sub> L<sup>-1</sup> (Phase III and V) presumably due to diffusion limitations. To assess whether  $r_{NOB,cycle}$  was suppressed only by DO limitation or also by NO<sub>2</sub><sup>-</sup> limitation,  $r_{i,cycle}$  were measured under non-limiting NO<sub>2</sub><sup>-</sup> concentrations. No increase in  $r_{NOB,cycle}$  was observed, confirming that DO rather than NO<sub>2</sub><sup>-</sup> was the limiting substrate for NOB in the biofilm (Fig. 2c, vertical black arrows in Phase V). As a result of the selective enrichment of AOB in the flocs, high NO<sub>2</sub><sup>-</sup> fluxes to the biofilm for AMX can be guaranteed at sufficiently low DO to suppress NOB activity in the biofilm.

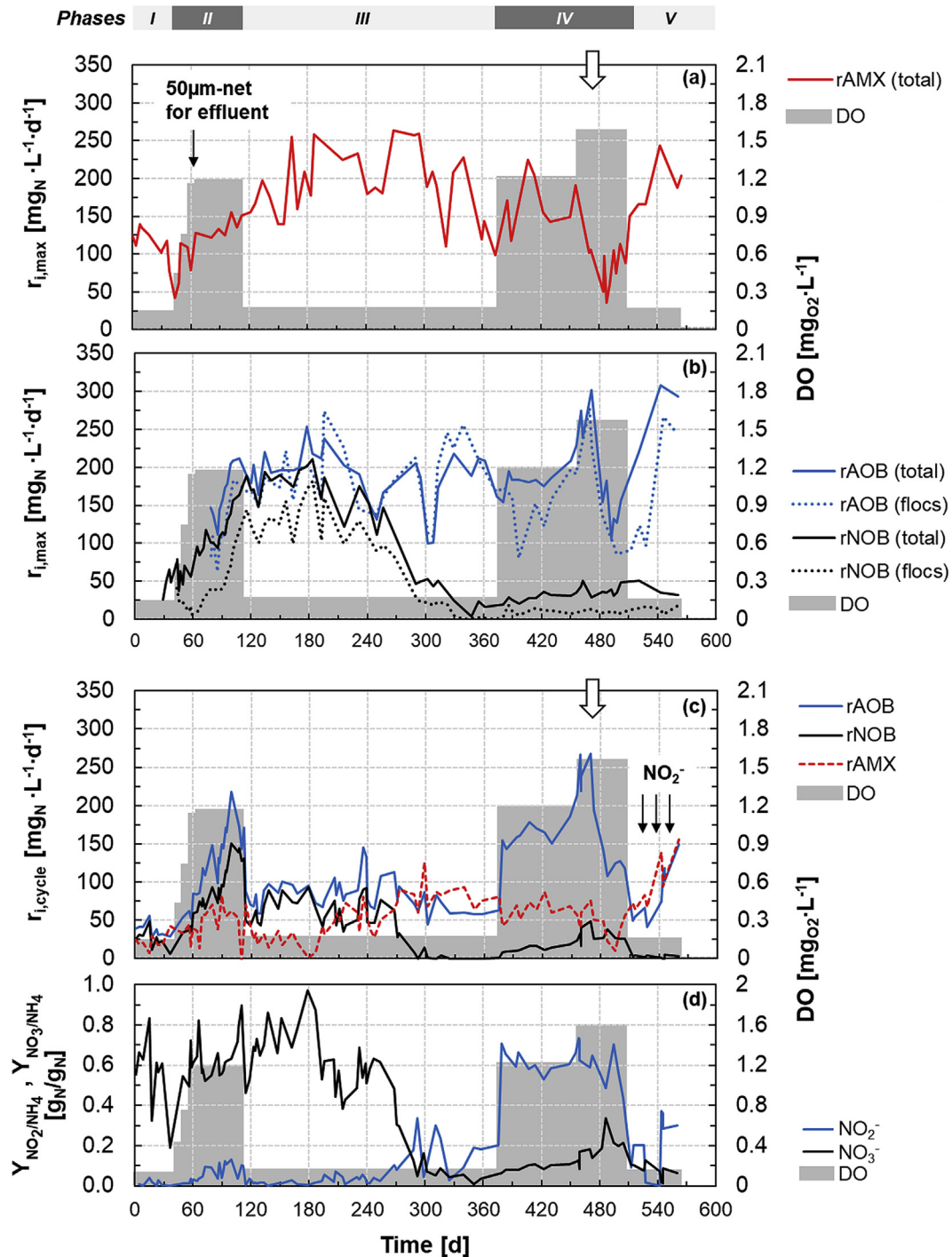


**Fig. 2.** Time series of the maximum ( $r_{i,max}$ ) and actual ( $r_{i,cycle}$ ) volumetric activities of AOB, NOB, and AMX in the hybrid MBBR. (a) Total maximum volumetric activities of AMX (the activity in the flocs was negligible throughout the experimental period). (b) Segregation of maximum volumetric activities of AOB and NOB: total biomass (biofilm and flocs) and floc fraction only. (c) Actual volumetric activities measured during the aerobic phase of an SBR cycle. Activities are expressed as follows: AOB,  $\text{mg}_{\text{NH}_4\text{-N}} \cdot \text{L}^{-1} \cdot \text{d}^{-1}$ ; NOB,  $\text{mg}_{\text{NO}_3\text{-N}} \cdot \text{L}^{-1} \cdot \text{d}^{-1}$ ; AMX,  $\text{mg}_{(\text{NH}_4\text{-N} + \text{NO}_2\text{-N})} \cdot \text{L}^{-1} \cdot \text{d}^{-1}$ . (d) Yields of  $\text{NO}_2^-$  and  $\text{NO}_3^-$  accumulated relative to the  $\text{NH}_4^+$  consumed during the aerobic phase. Shaded area: the average of the DO concentration measured during aeration over the representative periods. Vertical black arrows: in (a) time when floc retention was improved by filtering the effluent through a 50- $\mu\text{m}$ -mesh filter-bag; in (c) time when the volumetric activities during regular operation were measured under non-limiting nitrite concentrations. Vertical empty arrows: in (a, c) time of the prolonged rain event.

#### 4.1.5. Effluent quality

Overall, the wash-out of NOB from the flocs and the suppression of their activity in the biofilm at low DO, resulted in N-removals over  $88 \pm 4\%$  and a residual concentration of total N below  $3 \text{ mg}_\text{N} \text{ L}^{-1}$  ( $1.9 \pm 0.5 \text{ mg}_{\text{NH}_4\text{-N}} \text{ L}^{-1}$ ,  $0.3 \pm 0.2 \text{ mg}_{\text{NO}_2\text{-N}} \text{ L}^{-1}$ , and  $0.5 \pm 0.3 \text{ mg}_{\text{NO}_3\text{-N}} \text{ L}^{-1}$ ). This is the highest effluent quality reported so far for

mainstream PN/A systems (De Clippeleir et al., 2013; Gilbert et al., 2015; Laurenzi et al., 2016; Lotti et al., 2014). Moreover, the aerobic N-removal rates achieved ( $79 \pm 16 \text{ mg}_\text{N} \text{ L}^{-1} \text{ d}^{-1}$ ), at an HRT of  $11 \pm 2 \text{ h}$ , were comparable to those of conventional WWTP (Metcalf et al., 2013). The dynamics of influent and effluent concentrations are presented in Figure S3.



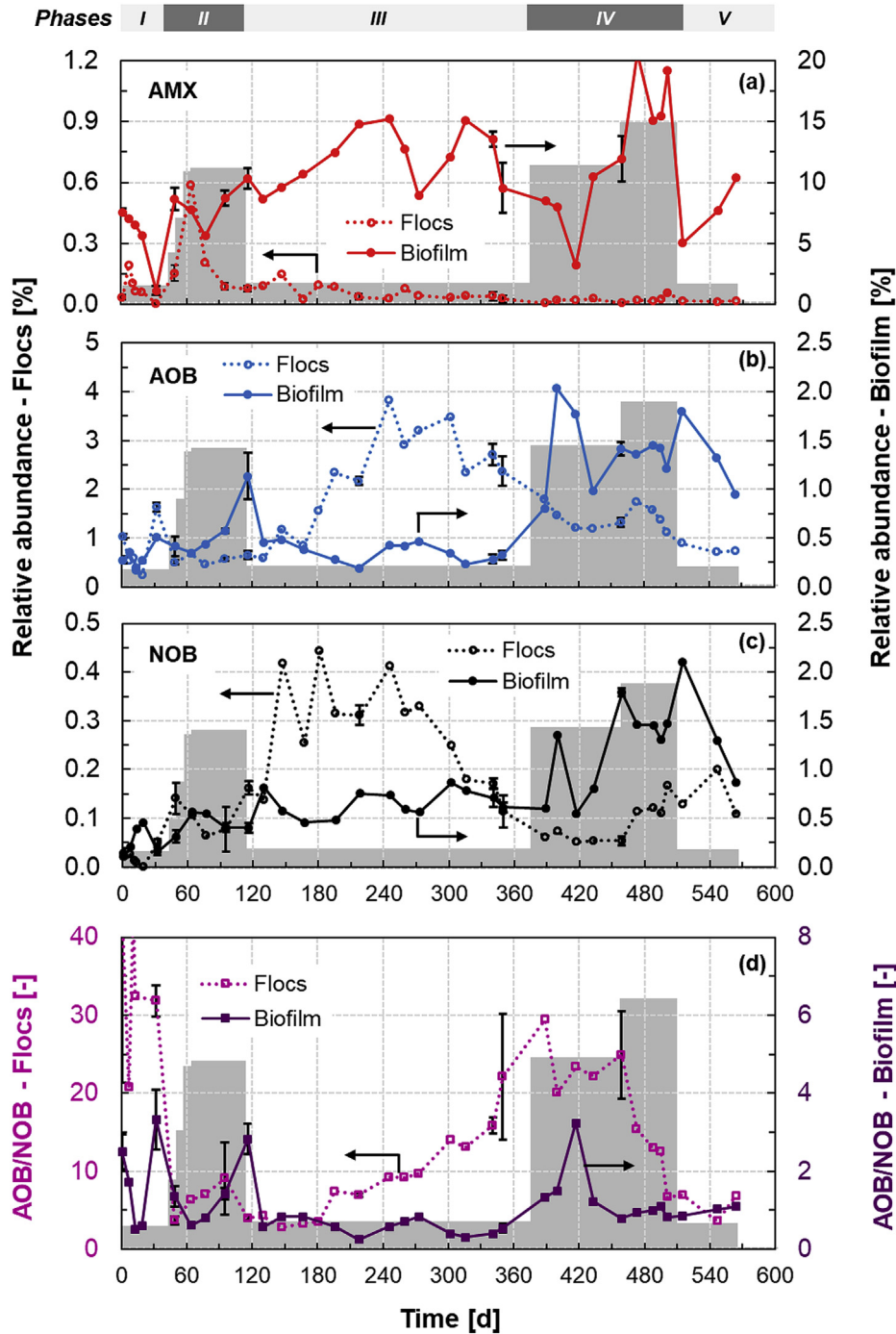


**Fig. 3.** Time series of the relative abundances of AMX (a), AOB (b), and NOB (c) in the flocs (left y-axis) and biofilm (right y-axis) as estimated by 16S rRNA gene-based amplicon sequencing analysis. The displayed values represent the sum of the relative abundances of all OTUs detected for each guild. For the time series of the single OTUs, see Fig. S4. (d) Time series of the dimensionless ratio between the relative abundances of AOB and NOB in the flocs ( $AOB/NOB - Flocs$ ) and biofilm ( $AOB/NOB - Biofilm$ ). Shaded area: average operational DO concentration over the representative periods (for values, see Fig. 2). Error bars: standard deviation of biological triplicates.

#### 4.2. Mathematical modelling of the hybrid MBBR

A simple dynamic model was developed to understand how the NOB concentration in the flocs ( $X_{NOB}$ ) respond to changes in DO, fraction of flocs removed per SBR cycle ( $f_{WAS}$ ), and maximum volumetric AMX activity in the biofilm ( $r_{AMX,max}$ ). To assess the impact of the individual control parameters four different scenarios were simulated (Table 3). The dynamics of  $X_{AOB}$  and  $X_{NOB}$ , and effluent N concentrations are presented in Fig. 4, and one cycle at

pseudo steady-state is shown for each scenario in Figure S5. The interdependences between the parameters and the impacts of substrate affinities are also discussed.

##### 4.2.1. Scenario 1 (baseline): high AOB and NOB enrichment in the flocs

A low initial concentration of  $1 \text{ mg}_{COD} \text{ L}^{-1}$  was set for  $X_{AOB}$  and  $X_{NOB}$ . Prolonged operation at  $1.5 \text{ mg}_{O2} \text{ L}^{-1}$  resulted in the enrichment of both AOB and NOB in the flocs (Fig. 4a), similar to

experimental observations during reactor operation (Phase II, Fig. 2). The pseudo steady-state  $X_{AOB}$  and  $X_{NOB}$  obtained in Scenario 1 were assumed as initial concentrations for the other scenarios.

#### 4.2.2. Scenario 2: the DO controls the selective washout of NOB from the flocs

The DO has a direct impact on the growth rate of both AOB and NOB (see process rates in Table 1). AOB and NOB are also equally exposed to washout, e.g. by removing a fraction of flocs at the end of each SBR cycle ( $f_{WAS}$ ). However, only the NOB growth rate is impacted by the competition for  $NO_2^-$  with the “ $NO_2$ -sink” represented by the AMX in the biofilm. This direct competition for  $NO_2^-$  between NOB and AMX leads to a difference in the actual growth rates of AOB and NOB (i.e.,  $\mu_{NOB} < \mu_{AOB}$ ) providing the basis for the selective NOB washout (i.e.,  $\mu_{NOB} < SRT^{-1} < \mu_{AOB}$ ).

The impact of a DO decrease to  $0.15 \text{ mg}_{O_2} \text{ L}^{-1}$  was assessed in Scenario 2 to reflect the experimental strategy (Phase III, Fig. 2). Under the imposed DO-limiting condition, and at the fixed  $f_{WAS}$ , only AOB could be maintained in the system while NOB were successfully washed out. High N-removals are achieved (84%; Fig. 4b, f). At the same time, due to the decreased AOB activity the HRT increases from 1.6 to 5.9 h (i.e. longer cycles are required to achieve the set effluent  $NH_4^+$  concentration). In terms of effluent concentrations, the reduction of the DO limits the aerobic activity (as was the case in the reactor, Fig. 2c) and results in the immediate reduction of  $NO_3^-$  (Fig. 4f).

The numerical results provide a mechanistic interpretation for the experimental observations: the sole reduction of the DO was sufficient to reduce the actual NOB growth rate below the minimum required to prevent their washout. Moreover, the simulations support the possibility to use DO to achieve the selective washout of NOB from the flocs.

#### 4.2.3. Scenario 3: increasing the fraction of flocs removed per cycle is an effective strategy to achieve selective NOB washout

Decreasing the DO might not always be a viable option at full scale, either because the operational DO is already low or the size of the installed aerators and blowers is not suitable (Joss et al., 2011). Conversely, the selective removal of the flocs from a hybrid MBBR, or of fine particles from a granular sludge system, may be a more feasible option, e.g., via a separate settler (Veuillet et al., 2014), hydrocyclone (Wett et al., 2015), or screen (Han et al., 2016). Simulations were run to assess the effectiveness of increasing the fraction of flocs removed at the end of each SBR cycle as a strategy to achieve the selective washout of NOB.

Numerical results suggest that successful NOB washout can indeed be achieved by increasing  $f_{WAS}$  while maintaining all other conditions unchanged. Under Scenario 3, only the  $f_{WAS}$  was increased to 1.7% and, as a result, NOB were selectively washed out at an SRT of 6.8 d (Fig. 4c). In this case, the actual NOB growth rate (function of DO and  $NO_2^-$  concentrations, Table 1) is no longer sufficient to compensate for the increased washout. Simultaneously, the significantly lower AOB concentrations maintained in the system result in higher HRT and thus reduced N-loads that can be treated at the same effluent quality (Eq. (7)). Nevertheless, in comparison to lowering the DO, increasing  $f_{WAS}$  allows a faster NOB washout. From a process control perspective, the proposed simulation examples highlight how in principle NOB can be washed out by only controlling the removal of the flocs.

#### 4.2.4. Scenario 4: variations of AMX activity in the biofilm - the “ $NO_2$ -sink” - have a direct impact on NOB concentration in the flocs

The NOB in the flocs compete for  $NO_2^-$  with the AMX enriched in the biofilm - the “ $NO_2$ -sink” - here represented by the maximum volumetric AMX activity ( $r_{AMX,max}$ ). Increasing  $r_{AMX,max}$ , i.e. the rate of  $NO_2^-$  consumption by AMX, reduces the bulk  $NO_2^-$  concentration

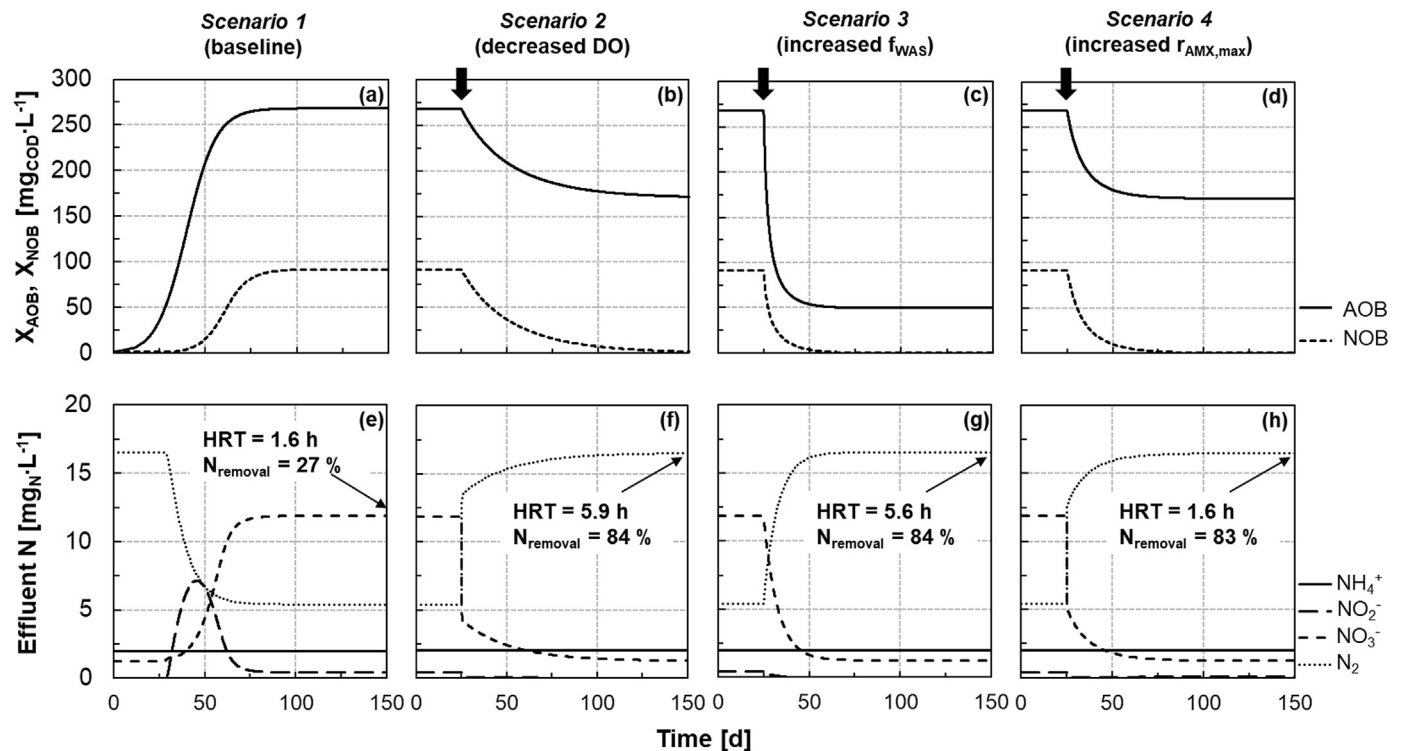


Fig. 4. Results from mathematical modelling of dynamics in concentrations of AOB ( $X_{AOB}$ ), NOB ( $X_{NOB}$ ), and effluent N towards the pseudo steady-state for the four scenarios detailed in Table 3. Pseudo steady-state in Scenario 1 is used as initial conditions for Scenarios 2, 3, and 4. Profiles of nitrogen species and biomass evolution during an SBR cycle at pseudo steady-state for the four scenarios are presented in Fig. S6. Vertical thick arrows: times when scenario-specific modification of operational conditions was implemented.

and consequently the actual NOB growth rate analogously to decreasing the DO.

The possibility of achieving complete and selective NOB washout from the flocs by increasing  $r_{AMX,max}$  was shown numerically. Under *Scenario 4*, the increase in  $r_{AMX,max}$  resulted in a higher  $NO_2^-$  consumption, and thus a stronger competition with NOB, which are successfully washed out (Fig. 4d). At the same time, simulations indicate that increasing  $r_{AMX,max}$  results in slightly lower AOB concentrations, as AMX reduce the  $NH_4^+$  available for AOB growth, with however minor implications in terms of HRT. As a result, a high N-removal is achieved while still maintaining a low HRT. The dynamics in effluent N concentrations are similar to *Scenario 2*. An immediate decrease of the  $NO_3^-$  concentration, due to the reduced  $NO_2^-$  available for NOB, is followed by a further progressive reduction as NOB are washed out (Fig. 4h).

At full scale, the maximum AMX activity can in principle be increased, e.g. by bio-augmentation from a sidestream PN/A process (Wett et al., 2015). On the other hand, a partial or complete inhibition of the AMX guild represents the opposite case where NOB may grow in the flocs due to the reduced competition for  $NO_2^-$ . Under such circumstances, increasing  $f_{WAS}$  and/or reducing the DO may be suitable operational strategies to prevent NOB proliferation, as will be discussed in the next section.

#### 4.2.5. Interdependent impacts of DO, $f_{WAS}$ , and $r_{AMX,max}$ on NOB, and the impact of substrates diffusion in the biofilm

To better understand the interdependence between the different control parameters, the pseudo steady-state concentrations of  $X_{AOB}$ ,  $X_{NOB}$  and effluent  $NO_3^-$  are shown in Fig. 5 as a function of different  $r_{AMX,max}$  and  $f_{WAS}$ . Two DO concentrations were simulated (0.15 and 1.5  $mg_{O_2} L^{-1}$ ), representative of the low and high DO experimental periods. The pseudo steady-state of the four scenarios discussed in the previous sections are highlighted.

$X_{NOB}$  and the effluent  $NO_3^-$  concentration decrease with increasing  $r_{AMX,max}$  (i.e. the competing “ $NO_2^-$ -sink”). For any given DO and  $f_{WAS}$ , there is a minimum  $r_{AMX,max}$  required for full NOB washout from the flocs (Fig. 5b, e).  $X_{AOB}$  also decrease with increasing  $r_{AMX,max}$ . In fact, by consuming  $NH_4^+$ , AMX reduce its availability for AOB growth (Fig. 5a, d). This effect disappears, and  $X_{AOB}$  stabilizes, as soon as the NOB are fully washed out. As a matter of fact, when present in the system, NOB consume  $NO_2^-$  and indirectly favour AOB by decreasing  $NH_4^+$  depletion by AMX. As an example, the case of partial AMX inhibition would be equivalent to moving horizontally to the left in Fig. 5: an increased  $X_{NOB}$  is to be expected unless e.g. DO is decreased or/and  $f_{WAS}$  is increased.

Additional simulations with a conservative ten-times higher value for both  $NH_4^+$  and  $NO_2^-$  affinity constants of AMX were run to assess the effects of substrate diffusion through the biofilm on the

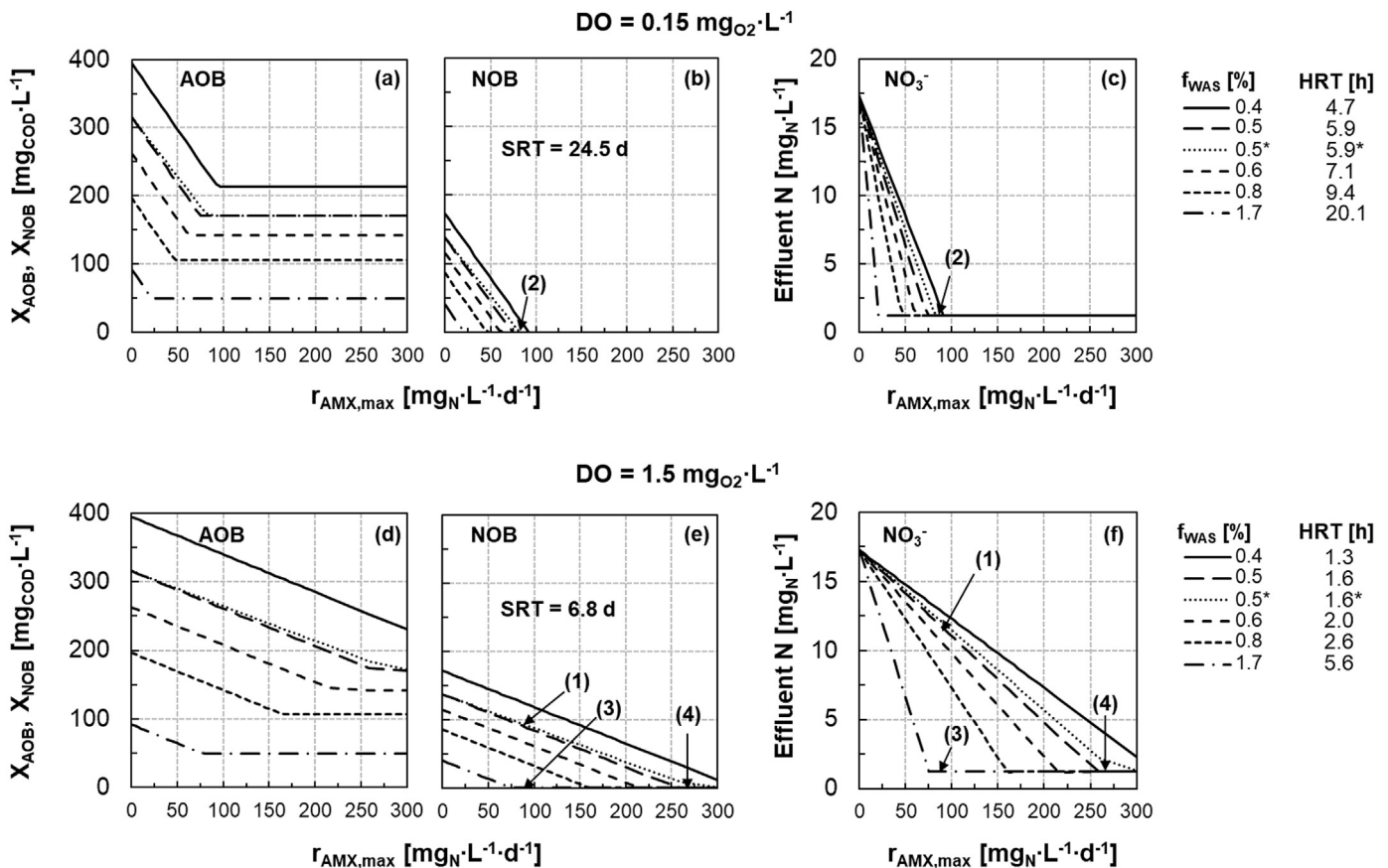


**Fig. 5.** Concentrations of AOB (a, d) and NOB (b, e) in the flocs under pseudo steady-state conditions modelled as a function of the maximum volumetric AMX activity ( $r_{AMX,max}$   $mg_{(NH_4+NO_2)-N} L^{-1} d^{-1}$ ) for two reference DO, 0.15 and 1.5  $mg_{O_2} L^{-1}$ . (c, f) Residual concentration of  $NO_3^-$  in the effluent at pseudo steady-state.  $NH_4^+$ ,  $NO_2^-$  and  $N_2$  concentrations are presented in Figure S5. The different lines represent different  $f_{WAS}$  values, as shown in the legend to the right of the figures. The resulting HRT for each  $f_{WAS}$  is also reported in the legend. Simulations were run with reference parameters shown in Table 2. Only for the case marked with (\*), the ammonium and nitrite affinity constants of AMX were increased by a factor of ten. Black arrows and numbers in parentheses: the four scenarios discussed in the text and presented in Fig. 4.

modelled pseudo steady-states. Only the case of  $f_{WAS}$  equal to 0.5 % was considered. As can be seen from Fig. 5, differences from the reference case (*i.e.* with unmodified affinity constants) are negligible. It is therefore deemed justified to neglect diffusion effects for the purpose of this work.

Overall, when interpreting the numerical results, it is important to consider the simplifying assumptions made in the modelling of the biofilm. AMX inhibition by oxygen was neglected, and the  $r_{AMX,max}$  was assumed to be the result of the active AMX in the anoxic layers of a deep biofilm. In addition, no NOB growth in the biofilm was considered. In this respect, it is worth noting that the nitrifying activity of NOB was shown experimentally to be completely suppressed at low DO. Additional simulations with more complex models, including biomass stratification and inhibition processes, are recommended here. Nevertheless, the simplified model allowed to identify the fundamental role played by the AMX-enriched biofilm (“NO<sub>2</sub>-sink”) in favouring the selective NOB washout from the flocs.

#### 4.2.6. The possibility of successful NOB washout from the flocs is not impaired by the values of the affinity constants

In solely biofilm PN/A systems, the ratio of the oxygen affinity constants,  $K_{O_2,NOB}/K_{O_2,AOB}$ , and the ratio of the NO<sub>2</sub> affinity constants,  $K_{NO_2,NOB}/K_{NO_2,AMX}$ , are reported as the main parameters controlling microbial competition (Brockmann and Morgenroth, 2010; Hao et al., 2002; Pérez et al., 2014; Picioreanu et al., 2016). For example, Hao et al. (2002) have reported that  $K_{O_2,NOB}/K_{O_2,AOB} > 0.2$  and  $K_{NO_2,NOB}/K_{NO_2,AMX} > 3$  is a required condition for successful NOB suppression in a biofilm system modelled at 30 °C.

In the present study, the sensitivity of the simulation results and the validity of the previously drawn conclusions was tested with respect to the ratios  $K_{O_2,NOB}/K_{O_2,AOB}$  and  $K_{NO_2,NOB}/K_{NO_2,AMX}$ . To ease the interpretation of the sensitivity analysis,  $K_{O_2,AOB}$  was maintained constant ( $0.6 \text{ mg}_{O_2} \text{ L}^{-1}$ ), and the  $K_{O_2,NOB}/K_{O_2,AOB}$  ratio was varied between 0.14 (Regmi et al., 2014) and 2.00 (Pérez et al., 2014) by changing  $K_{O_2,NOB}$  (Table S1). Simulations were run for the two reference DO of 0.15 and  $1.5 \text{ mg}_{O_2} \text{ L}^{-1}$ , and a fixed  $f_{WAS}$  of 0.5 %. The pseudo steady-state  $X_{NOB}$  and effluent NO<sub>2</sub> concentrations are displayed as a function of  $K_{O_2,NOB}/K_{O_2,AOB}$  in Fig. 6. An overview of  $X_{AOB}$  and  $X_{NOB}$ , and the effluent concentrations of the dissolved N species, is presented in Fig. S8.

At a low DO ( $0.15 \text{ mg}_{O_2} \text{ L}^{-1}$ ), the value of  $K_{O_2,NOB}/K_{O_2,AOB}$  determines the mechanisms controlling NOB washout. On the one hand, for values of  $K_{O_2,NOB}/K_{O_2,AOB} < 1$ , low NO<sub>2</sub> concentrations are modelled (*i.e.* rapidly consumed by NOB and AMX), and the competition with AMX for NO<sub>2</sub> is the dominant mechanism controlling NOB washout. Increasing  $r_{AMX,max}$  results in lower NOB pseudo steady-state concentrations (Fig. 6a). Importantly, NOB are successfully washed out in the model even in the extreme case of  $K_{O_2,NOB}/K_{O_2,AOB} = 0.14$  (Regmi et al., 2014), which would make their control challenging in solely biofilm systems (Brockmann and Morgenroth, 2010; Hao et al., 2002; Pérez et al., 2014). On the other hand, for higher values ( $K_{O_2,NOB}/K_{O_2,AOB} > 1$ ), DO limitation starts to play an important role. Due to the reduced NOB growth rate, lower NOB concentrations can be sustained in the system, and NO<sub>2</sub> accumulates if the AMX activity is not sufficiently high (Fig. 6b). Interestingly, for large  $K_{O_2,NOB}$  ( $K_{O_2,NOB}/K_{O_2,AOB} = 2.00$ ), NOB are washed out from the system even in the absence of AMX

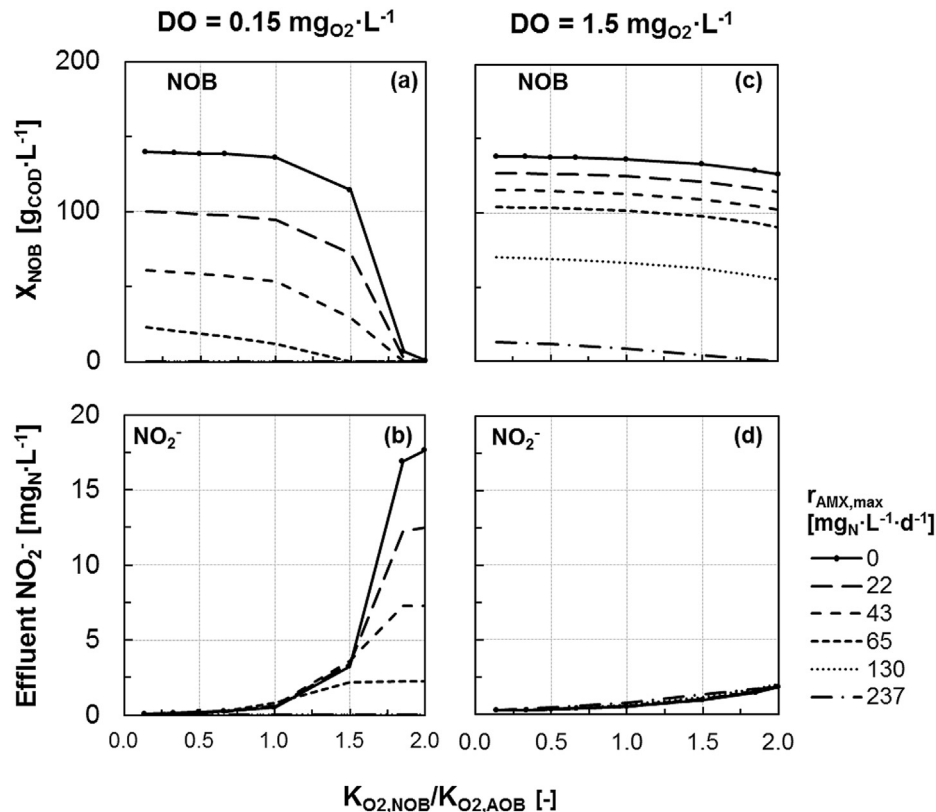


**Fig. 6.** Sensitivity analysis. Impact of different  $K_{O_2,NOB}/K_{O_2,AOB}$  on simulated NOB concentrations at pseudo steady-state (a, c) and corresponding effluent NO<sub>2</sub> concentrations (b, d) for the two reference DO ( $0.15$  and  $1.5 \text{ mg}_{O_2} \text{ L}^{-1}$ ).  $K_{O_2,NOB}/K_{O_2,AOB} = 0.67$  is the reference case (see Table 2). The values of the oxygen affinities for NOB and AOB and their ratio are presented in Table S1. In the simulations, an  $f_{WAS}$  of 0.5% was assumed. All concentrations of  $X_{AOB}$  and effluent N species at pseudo steady-state are presented in Figure S8.  $r_{AMX,max}$  is expressed as  $\text{mg}_{(NH_4+NO_2)-N} \text{ L}^{-1} \text{ d}^{-1}$ .



and despite high  $\text{NO}_2^-$  accumulation. In this case, the actual NOB growth rate is not sufficient to maintain them in the system at the cycle length set by AOB and the imposed  $f_{\text{WAS}}$  (Eq. (7)). Importantly, if  $r_{\text{AMX,max}}$  is sufficiently high (e.g.  $> 65 \text{ mg}_\text{N} \text{ L}^{-1} \text{ d}^{-1}$ ), the NOB washout does not depend on  $K_{\text{O}_2,\text{NOB}}/K_{\text{O}_2,\text{AOB}}$ .

At a high DO ( $1.5 \text{ mg}_\text{O}_2 \text{ L}^{-1}$ ), NOB washout is less sensitive to the value of  $K_{\text{O}_2,\text{NOB}}/K_{\text{O}_2,\text{AOB}}$ , and the competition for  $\text{NO}_2^-$  with AMX is the dominant mechanism controlling NOB washout (Fig. 6c). Nevertheless, in analogy to the low DO case,  $\text{NO}_2^-$  accumulation occurs for high values of  $K_{\text{O}_2,\text{NOB}}/K_{\text{O}_2,\text{AOB}}$ . Taken together, these results provide a mechanistic hypothesis to explain the seemingly contradictory experimental observations during Phase IV (Fig. 2), when only limited NOB enrichment was observed in the flocs despite high DO and pronounced  $\text{NO}_2^-$  accumulation. In general, higher  $r_{\text{AMX,max}}$  are required for NOB washout (e.g.,  $> 237 \text{ mg}_\text{N} \text{ L}^{-1} \text{ d}^{-1}$ ) compared to the case at low DO.

In terms of  $\text{NO}_2^-$  affinity constants,  $K_{\text{NO}_2,\text{NOB}}$  was decreased from a usually assumed value 100 times higher than  $K_{\text{NO}_2,\text{AMX}}$  (Hao et al., 2002; Pérez et al., 2014) to a value of 0.1  $K_{\text{NO}_2,\text{AMX}}$  (Figure S9). Decreasing  $K_{\text{NO}_2,\text{NOB}}$  increases the competitive advantage of NOB over AMX and results in higher  $X_{\text{NOB}}$  at pseudo steady-state for any given  $r_{\text{AMX,max}}$ . Nevertheless, within the broad range of values tested, NOB washout can always be achieved provided that a sufficiently high  $r_{\text{AMX,max}}$  is present (Fig. S9).

In summary, this work strongly support the increased operational flexibility offered by hybrid systems, as compared to solely biofilm systems, for the control of NOB under mainstream conditions. In fact, irrespective of the values chosen for the affinity constants, it is in principle always possible to control the selective pressure on NOB via DO,  $f_{\text{WAS}}$ , and/or  $r_{\text{AMX,max}}$ , and achieve their complete washout.

## 5. Conclusions

This study aimed at understanding the mechanisms underlying microbial competition and the control of NOB in hybrid PN/A reactors. To this end, a hybrid MBBR was operated under mainstream conditions and a simple mathematical model of the system was developed. Experimentally, AMX were shown to enrich in the biofilm while AOB and NOB grew preferentially in the flocs. AMX are retained in the biofilm independent of floc removal and they act as a “ $\text{NO}_2^-$ -sink”. Conversely, AOB and NOB are maintained in the flocs only if their actual growth rates is larger than the imposed washout (i.e., if  $\mu > \text{SRT}^{-1}$ ).

- The key mechanisms for selectively washing out NOB from the system are maintaining a sufficiently low SRT for the flocs and limiting  $\text{NO}_2^-$  bulk phase concentrations by means of the AMX “ $\text{NO}_2^-$ -sink”. AOB growth rates are not affected by  $\text{NO}_2^-$  bulk phase concentrations allowing reactor operation with selective washout of NOB while keeping AOB.
- Experimental results and numerical simulations showed that, for an imposed fraction of flocs removed per SBR cycle or given SRT, NOB can be selectively washed out by decreasing the DO-setpoint, e.g., from 1.2 to  $0.17 \text{ mg}_\text{O}_2 \text{ L}^{-1}$ . In this case, while both AOB and NOB actual growth rates decrease; due to the concurrent  $\text{NO}_2^-$ -limitation only NOB growth rate is reduced below the washout threshold i.e.,  $\mu_{\text{NOB}} < \text{SRT}^{-1} < \mu_{\text{AOB}}$ .
- In analogy, for a given DO-setpoint, simulations indicated that selective NOB washout can be achieved also by increasing the fraction of flocs removed: the actual NOB growth rate remains unaffected but is no longer sufficient to compensate for the increased washout.
- Moreover, differently from pure biofilm systems where NOB suppression relies on a larger oxygen affinity of AOB than NOB,

modelling results suggest that it is in principle always possible to selectively wash out NOB by controlling the DO-setpoint and/or the flocs removal provided AMX act as “ $\text{NO}_2^-$ -sink” in the biofilm.

Ultimately, this study demonstrates the high operational flexibility, in terms of variables that can be easily controlled by operators, offered by hybrid systems for the control of NOB in mainstream PN/A applications.

## Acknowledgements

This study was funded by the European Research Council ERC via the ATHENE project (grant agreement 267897). ML was partially supported by a Marie Skłodowska-Curie Individual Fellowship (MixAmox project; grant agreement 752992). We sincerely thank Kai Udert, Nicolas Derlon and Fabrizio Sabba for valuable discussions, Marco Kipf for his support in the laboratory, Brian Sinnet for the particle size analysis, and Claudia Baenninger-Werffeli, Sylvia Richter, and Karin Rottermann for their assistance with the physicochemical analyses of all the samples.

## Appendix A. Supplementary data

Supplementary data to this article can be found online at <https://doi.org/10.1016/j.watres.2018.12.051>.

## References

- Anthonisen, A.C., Loehr, R.C., Prakasam, T.B., Srinath, E.G., 1976. Inhibition of nitrification by ammonia and nitrous acid. *J. Water Pollut. Control Fed.* 48 (5), 835–852.
- APHA, 2005. Standard Methods for the Examination of Water and Wastewater, Washington, D.C.
- Blackburne, R., Vadivelu, V.M., Yuan, Z., Keller, J., 2007. Kinetic characterisation of an enriched Nitrospira culture with comparison to Nitrobacter. *Water Res.* 41 (14), 3033–3042.
- Brockmann, D., Morgenroth, E., 2010. Evaluating operating conditions for out-competing nitrite oxidizers and maintaining partial nitrification in biofilm systems using biofilm modeling and Monte Carlo filtering. *Water Res.* 44 (6), 1995–2009.
- Corbala-Robles, L., Picioreanu, C., van Loosdrecht, M.C., Perez, J., 2016. Analysing the effects of the aeration pattern and residual ammonium concentration in a partial nitrification-anammox process. *Environ. Technol.* 37 (6), 694–702.
- De Clippeleir, H., Vlaeminck, S.E., De Wilde, F., Daeninck, K., Mosquera, M., Boeckx, P., Verstraete, W., Boon, N., 2013. One-stage partial nitrification/anammox at  $15^\circ\text{C}$  on pretreated sewage: feasibility demonstration at lab-scale. *Appl. Microbiol. Biotechnol.* 97 (23), 10199–10210.
- Fux, C., Huang, D., Monti, A., Siegrist, H., 2004. Difficulties in maintaining long-term partial nitrification of ammonium-rich sludge digester liquids in a moving-bed biofilm reactor (MBBR). *Water Sci. Technol.* 49 (11–12), 53–60.
- Gilbert, E.M., Agrawal, S., Schwartz, T., Horn, H., Lackner, S., 2015. Comparing different reactor configurations for Partial Nitrification/Anammox at low temperatures. *Water Res.* 81, 92–100.
- Han, M., Vlaeminck, S.E., Al-Omari, A., Wett, B., Bott, C., Murthy, S., De Clippeleir, H., 2016. Uncoupling the solids retention times of flocs and granules in mainstream deammonification: a screen as effective out-selection tool for nitrite oxidizing bacteria. *Bioresour. Technol.* 221, 195–204.
- Hao, X., Heijnen, J.J., van Loosdrecht, M.C.M., 2002. Sensitivity analysis of a biofilm model describing a one-stage completely autotrophic nitrogen removal (CANON) process. *Biotechnol. Bioeng.* 77 (3), 266–277.
- Hellinga, C., Schellen, A.A.J.C., Mulder, J.W., van Loosdrecht, M.C.M., Heijnen, J.J., 1998. The SHARON process: an innovative method for nitrogen removal from ammonium-rich waste water. *Water Sci. Technol.* 37 (9), 135–142.
- Hubaux, N., Wells, G., Morgenroth, E., 2015. Impact of coexistence of flocs and biofilm on performance of combined nitrification-anammox granular sludge reactors. *Water Res.* 68, 127–139.
- Isanta, E., Reino, C., Carrera, J., Perez, J., 2015. Stable partial nitrification for low-strength wastewater at low temperature in an aerobic granular reactor. *Water Res.* 80, 149–158.
- Joss, A., Derlon, N., Cyprien, C., Burger, S., Szivák, I., Traber, J., Siegrist, H., Morgenroth, E., 2011. Combined nitrification-anammox: advances in understanding process stability. *Environ. Sci. Technol.* 45 (22), 9735–9742.
- Jubany, I., Lafuente, J., Baeza, J.A., Carrera, J., 2009. Total and stable washout of nitrite oxidizing bacteria from a nitrifying continuous activated sludge system using automatic control based on Oxygen Uptake Rate measurements. *Water Res.* 43

- (11), 2761–2772.
- Lackner, S., Gilbert, E.M., Vlaeminck, S.E., Joss, A., Horn, H., van Loosdrecht, M.C.M., 2014. Full-scale partial nitrification/anammox experiences - an application survey. *Water Res.* 55, 292–303.
- Laureni, M., Falás, P., Robin, O., Wick, A., Weissbrodt, D.G., Nielsen, J.L., Ternes, T.A., Morgenroth, E., Joss, A., 2016. Mainstream partial nitrification and anammox: long-term process stability and effluent quality at low temperatures. *Water Res.* 101, 628–639.
- Laureni, M., Weissbrodt, D.G., Szivak, I., Robin, O., Nielsen, J.L., Morgenroth, E., Joss, A., 2015. Activity and growth of anammox biomass on aerobically pre-treated municipal wastewater. *Water Res.* 80, 325–336.
- Leix, C., Drewes, J.E., Koch, K., 2016. The role of residual quantities of suspended sludge on nitrogen removal efficiency in a deammonifying moving bed biofilm reactor. *Bioresour. Technol.* 219, 212–218.
- Liu, G., Wang, J., 2013. Long-term low DO enriches and shifts nitrifier community in activated sludge. *Environ. Sci. Technol.* 47 (10), 5109–5117.
- Lotti, T., Kleerebezem, R., Hu, Z., Kartal, B., de Kreuk, M., van Erp Taalman Kip, C., Kruit, J., Hendrickx, T.L.G., van Loosdrecht, M.C.M., 2015. Pilot-scale evaluation of anammox-based mainstream nitrogen removal from municipal wastewater. *Environ. Technol.* 36 (9), 1167–1177.
- Lotti, T., Kleerebezem, R., Hu, Z., Kartal, B., Jetten, M.S.M., van Loosdrecht, M.C.M., 2014. Simultaneous partial nitrification and anammox at low temperature with granular sludge. *Water Res.* 66, 111–121.
- Malovanyy, A., Trela, J., Plaza, E., 2015. Mainstream wastewater treatment in integrated fixed film activated sludge (IFAS) reactor by partial nitrification/anammox process. *Bioresour. Technol.* 198, 478–487.
- Metcalfe, Eddy, I., Tchobanoglous, G., Stensel, H.D., Tsuchihashi, R., Burton, F., 2013. *Wastewater Engineering: Treatment and Resource Recovery*. McGraw-Hill Education.
- Morgenroth, E., 2008. In: Henze, M., van Loosdrecht, M.C.M., Ekama, G., Brdjanovic, D. (Eds.), *Biological Wastewater Treatment - Principles, Modelling, and Design*. IWA Publishing, London.
- Park, H., Sundar, S., Ma, Y., Chandran, K., 2014. Differentiation in the microbial ecology and activity of suspended and attached bacteria in a nitrification-anammox process. *Biotechnol. Bioeng.* 112 (2), 272–279.
- Pérez, J., Lotti, T., Kleerebezem, R., Picioreanu, C., van Loosdrecht, M.C., 2014. Out-competing nitrite-oxidizing bacteria in single-stage nitrogen removal in sewage treatment plants: a model-based study. *Water Res.* 66, 208–218.
- Picioreanu, C., Pérez, J., van Loosdrecht, M.C.M., 2016. Impact of cell cluster size on apparent half-saturation coefficients for oxygen in nitrifying sludge and biofilms. *Water Res.* 106, 371–382.
- Poot, V., Hoekstra, M., Geleijnse, M.A., van Loosdrecht, M.C., Perez, J., 2016. Effects of the residual ammonium concentration on NOB repression during partial nitrification with granular sludge. *Water Res.* 106, 518–530.
- Regmi, P., Miller, M.W., Holgate, B., Bunce, R., Park, H., Chandran, K., Wett, B., Murthy, S., Bott, C.B., 2014. Control of aeration, aerobic SRT and COD input for mainstream nitrification/denitrification. *Water Res.* 57, 162–171.
- Rittmann, B.E., McCarty, P.L., 2001. *Environmental Biotechnology: Principles and Applications*. McGraw-Hill Education.
- Shi, Y., Wells, G., Morgenroth, E., 2016. Microbial activity balance in size fractionated suspended growth biomass from full-scale sidestream combined nitrification-anammox reactors. *Bioresour. Technol.* 218, 38–45.
- Siegrist, H., Salzgeber, D., Eugster, J., Joss, A., 2008. Anammox brings WWTP closer to energy autarky due to increased biogas production and reduced aeration energy for N-removal. *Water Sci. Technol.* 57 (3), 383–388.
- Slikkers, A.O., Haaijer, S.C., Stafsnes, M.H., Kuenen, J.G., Jetten, M.S., 2005. Competition and coexistence of aerobic ammonium- and nitrite-oxidizing bacteria at low oxygen concentrations. *Appl. Microbiol. Biotechnol.* 68 (6), 808–817.
- Speth, D.R., In 't Zandt, M.H., Guerrero-Cruz, S., Dutilh, B.E., Jetten, M.S., 2016. Genome-based microbial ecology of anammox granules in a full-scale wastewater treatment system. *Nat. Commun.* 7, 11172.
- Strous, M., Heijnen, J.J., Kuenen, J.G., Jetten, M.S.M., 1998. The sequencing batch reactor as a powerful tool for the study of slowly growing anaerobic ammonium-oxidizing microorganisms. *Appl. Microbiol. Biotechnol.* 50 (5), 589–596.
- Takács, I., Stricker, A.-E., Achleitner, S., Barrie, A., Rauch, W., Murthy, S., 2008. Do you know your sludge age? *Proc. Water Environ. Feder.* 2008 (13), 3639–3655.
- van Loosdrecht, M.C.M., Brdjanovic, D., 2014. Water treatment. Anticipating the next century of wastewater treatment. *Science* 344 (6191), 1452–1453.
- Veuillet, F., Lacroix, S., Bausseron, A., Gonidec, E., Ochoa, J., Christensson, M., Lemaire, R., 2014. Integrated fixed-film activated sludge ANITAMox process - a new perspective for advanced nitrogen removal. *Water Sci. Technol.* 69 (5), 915–922.
- Vlaeminck, S.E., Terada, A., Smets, B.F., De Clippeleir, H., Schaubroeck, T., Bolca, S., Demeestere, L., Mast, J., Boon, N., Carballa, M., Verstraete, W., 2010. Aggregate size and architecture determine microbial activity balance for one-stage partial nitrification and anammox. *Appl. Environ. Microbiol.* 76 (3), 900–909.
- Volcke, E.I., Picioreanu, C., De Baets, B., van Loosdrecht, M.C., 2012. The granule size distribution in an anammox-based granular sludge reactor affects the conversion-implications for modeling. *Biotechnol. Bioeng.* 109 (7), 1629–1636.
- Wells, G.F., Shi, Y., Laureni, M., Rosenthal, A., Szivak, I., Weissbrodt, D.G., Joss, A., Buergermann, H., Johnson, D.R., Morgenroth, E., 2017. Comparing the resistance, resilience, and stability of replicate moving bed biofilm and suspended growth combined nitrification-anammox reactors. *Environ. Sci. Technol.* 51 (9), 5108–5117.
- Wett, B., Podmirseg, S.M., Gómez-Brandón, M., Hell, M., Nyhuis, G., Bott, C., Murthy, S., 2015. Expanding DEMON sidestream deammonification Technology towards mainstream application. *Water Environ. Res.* 87 (12), 2084–2089.
- Winkler, M.K.H., Kleerebezem, R., Kuenen, J.G., Yang, J., van Loosdrecht, M.C.M., 2011. Segregation of biomass in cyclic anaerobic/aerobic granular sludge allows the enrichment of anaerobic ammonium oxidizing bacteria at low temperatures. *Environ. Sci. Technol.* 45 (17), 7330–7337.
- Wiesmann, U., 1994. Biological nitrogen removal from wastewater. *Adv. Biochem. Eng. Biotechnol.* 51, 113–154.
- WPO, 1998. Water Protection Ordinance of 28 October 1998 (814.201). UNECE, Geneva.